Turbulent Diffusion of a Reacting Wake

WILMOT H. WEBB* AND LESLIE A. HROMAS†
TRW Space Technology Laboratories, Redondo Beach, Calif.

Properties of the nonequilibrium hypersonic turbulent wake have been calculated from an integral solution for the coupled diffusion of mass and energy. Emphasis is placed on 1) a comparison of a slender body calculation from the present simple method with results obtained for the same case by more advanced mathematical techniques such as finite-difference methods, 2) new blunt body results in which the reacting inviscid flow is entrained by the turbulent inner wake, 3) the effect of contaminants on both slender and blunt-body wakes, and 4) a comparison of the present calculations with ballistic range measurements for wake velocity and electron density. The analysis described herein is a direct extension of the method proposed by Lees and Hromas for the equilibrium wake. By using two parameters to describe the distribution of each species in the wake, the integral method applied here provides sufficient generality to permit the determination of a variety of reacting turbulent flow fields, yet retains the basic numerical simplicity inherent in integral techniques. In the chemical kinetic model studied, particular attention is paid to the processes of far downstream electron decay, and, for the first time, combined atomic and molecular oxygen attachment, charge neutralization, and charge exchange reactions are considered. In addition, some new explicit solutions are given that provide useful criteria in evaluating the respective roles of chemical reactions and diffusion in the wake. These solutions are useful in obtaining scaling laws, which are not always evident in detailed computer calculations.

Nomenclature

$B(x)$ = $[h(0, x) - h_f(x)]/h_\infty$
C_D = wake drag coefficient
d = body diameter
g = inviscid enthalpy radial distribution function
G = turbulent radial distribution function
h = thermal and chemical enthalpy
H = $h_L(0)/h_\infty - 1$
H_s = freestream stagnation enthalpy
k = reaction rate
K = universal diffusion constant
m = two-dimensional ($m=0$) or axisymmetric ($m=1$) exponent
M = Mach number, also reaction catalyst
$\mathfrak{M}$ = molecular weight
n_i = species number density
p = pressure
R_0 = gas constant
T = temperature
u = axial velocity
v = radial velocity
x = axial coordinate
y = radial coordinate
Y = Howarth-Dorodnitsyn scale
α_i = species mass fraction
β_i = $[\alpha_i(0, x) - \alpha_{if}]/[\alpha_{i0} - \alpha_{if}]$
γ_∞ = specific heat ratio
ϵ = turbulent diffusivity
ρ = density
θ_i = Y_T/Y_{si}
$\dot{\omega}_i$ = species production term $d(\alpha_i\rho)/dt$

Subscripts

A = atomic species
a = attachment rate
b = backward reaction rate
e = electrons
E = equilibrium value
f = edge of wake; also forward reaction rate
i = ith species
L = inviscid flow quantity
0 = quantity at wake origin, $x = x_0$
r = recombination rate
s = species quantity
T = turbulent flow quantity
∞ = freestream value

Introduction

THE trails behind meteors entering the atmosphere have long been of interest to astronomical observers.[1] Recently, new emphasis has been placed on the analysis of reentry wakes because of the problems of detection of, and communication with, military and space vehicles. Over a major portion of an atmospheric re-entry flight, the wake is turbulent. At present, a number of analyses of the chemically frozen or equilibrium wake are available. For example, Refs. 2 and 3 treat the case where the enthalpy in the external stream is uniform, whereas Refs. 4 and 5 take into account the entrainment of vorticity in the external flow by the growth of the turbulent core.

However, chemical equilibrium prevails over only the very lowest part of the re-entry trajectory. Thus more recent attention has been given to the reacting turbulent wake. Initially, Lees[6] gave a simple integral solution for electron concentration in the flow with a given temperature distribution. Next, Bloom and Steiger[7] reported some early results of an integral solution for the nonequilibrium laminar and turbulent wake of a slender body. A single parameter was used to represent each chemical species, and the species radial distribution was related to the velocity distribution (Crocco relation).

A simple version of the technique used herein was then given by the present authors in Ref. 8, where sample calculations were presented for the wake of a slender body. The present work extends these early results to blunt-body flows, and includes results for the contaminated wakes of both

Presented as Preprint 64-42 at the AIAA Aerospace Sciences Meeting, New York, January 20–22, 1964; revision received February 16, 1965. This research was supported jointly by the Air Force Ballistic Missile Division, Air Research and Development Command, U. S. Air Force under Contract No. AF04(694)-440 and by the Advanced Research Projects Agency and was administered by the Air Force Ballistic Missile Division, Air Research and Development Command, U. S. Air Force under Contract No. AF04(694)-439. The authors gratefully acknowledge their stimulating discussions with Lester Lees of the California Institute of Technology and with A. G. Hammitt of Space Technology Laboratories.

* Member of the Technical Staff. Member AIAA.
† Assistant Manager of the Aerophysics Department, Research. Member AIAA.

blunt and slender bodies. In addition, comparisons with ballistic range measurements of wake velocity and electron concentration and comparisons with detailed finite-difference calculations of other workers are also given.

In an analysis subsequent to Refs. 1–8, Lien, Erdos, and Pallone[9] have applied a refined integral method for slender bodies in which both the momentum and species equations are employed as well as the energy equation. Wake axis values of the flow variables and a profile shape factor are used as parameters, and, as in the original Lees-Hromas method and its present extension, integrated conservation equations along with the axis equations are then used to evaluate the parameters. In the method of Lien et al., the wake width in Howarth-Dorodnitsyn coordinates is assumed to be given. The advantage of this refined solution for the turbulent wake over the present approach is in the inclusion of a variable velocity, which is important in the first 0–10 diam. On the other hand, the present approach does not require an empirical wake growth and allows for a radial variation in inviscid enthalpy.‡ Reference 9 also gives a nonequilibrium analysis for the laminar wake, using a strip method where five strips are usually used (one strip is used in the usual integral method). Zeiberg and Bleich[10] have compared a finite-difference calculation with results for the laminar wake from the earlier integral method solution of Bloom and Steiger.[7] Appreciable differences for the laminar wake were found between the finite-difference solution and the integral solution of Ref. 7. The effect of different diffusivity laws for the turbulent wake was also examined in Ref. 10, and large deviations were found among the results. The finite-difference method is certainly the most general, and a primary result of the present paper is a comparison of the present method with more elaborate numerical methods, such as those of Ref. 10. It should be noted that, in the detailed finite-difference solution, the turbulent diffusivity must be specified everywhere in the turbulent wake. It is not always straightforward to do this; even the concept of gradient diffusion is not clear at the edge of the wake.

Except for the calculation by the present authors in Ref. 8, none of the nonequilibrium results obtained by the methods discussed included a variable inviscid enthalpy field, i.e., they are all effectively slender body results.§ However, Lin and Hayes[11] have compared the so-called random inviscid convection model with a simple one-dimensional calculation for the reacting turbulent wake of a blunt body. The random convection model ignores the fundamental nonlinear interaction of turbulent eddies which is usually responsible for the relatively efficient mixing of a turbulent flow. Flow properties for the turbulent wake in their model are obtained by averaging local inviscid properties over a specified wake boundary (which is obtained from experimental evidence, or from a homogeneous mixing model calculation). On the other hand, the homogeneous model assumes that the entrained flow adopts the local turbulent structure instantaneously. The actual physical case may well lie somewhere in between the limiting cases discussed by Lin and Hayes. However, the well-known results of Townsend[12] for incompressible wakes indicate that, for the far wake, the homogeneous mixing model is a good representation,[5] and this model is adopted here. A resolution of this question for the hypersonic wake must await detailed experimental studies.

In the Lees-Hromas model, the turbulent enthalpy-excess trail is represented by the peak (axis) enthalpy level and by the lateral extent (width) of the trail. Although the velocity and stagnation enthalpy in a turbulent wake are nearly uniform after a short distance downstream,[5] a large static enthalpy excess trail persists for a hypersonic flow. For this reason, the enthalpy conservation equation is used to calculate the growth of the wake in the Lees-Hromas method. The velocity is assumed constant wherever it appears directly rather than as a difference across the wake. The essential simplicity of this model is retained herein by representing each species concentration by its axis value and by a characteristic profile width parameter. Just as for the enthalpy, the species are assumed to spread rapidly into an inhomogeneous inviscid flow with a mass diffusivity equal to the conductivity. The turbulent wake thus grows across streamlines of the inviscid flow and engulfs the species and energy contained in that flow. For blunt bodies, such as meteors, or for conical bodies of high cone angle, a significant part of the inviscid flow field external to the turbulent wake, but near the body, is also reacting. Therefore, the wake intercepts streamlines along which dissociation and ionization processes have occurred. On the other hand, for more slender bodies, the external flow is homogeneous with respect to species concentration, although still possessing a variable enthalpy in the radial direction. For this simpler case, only reactions in the wake itself need be considered.

To obtain the variation of the species concentrations at the axis and of the profile scale parameters with downstream distance, the species diffusion equations, including chemical kinetic terms, are integrated across the wake and, in addition, are satisfied along the wake axis. Two first-order differential equations result for each species in the wake, and these equations may be solved readily with the aid of a digital computer through a marching technique. It is also possible, by suitable simplifying assumptions, to obtain approximate but explicit solutions for several chemical processes of interest in the wake. A consideration of these solutions yields rough estimates of the relative extent of diffusion and chemical kinetic effects and suggests the range of applicability of scaling parameters.

In the chemical kinetic model studied, particular attention is given to the ion-electron reactions involved in the electron decay process. The influence of molecular and atomic oxygen attachment and associated neutralization and charge exchange reactions has been included in the study. As far as the authors are aware, previous chemical kinetic studies of wakes have not considered these attachment and charge exchange mechanisms jointly.

When complete solutions are obtained for the (laminar or turbulent) viscous-inviscid interaction problem in the base flow region and near wake,¶ a valid initial condition will then be available for the far-wake calculation, and the results of the near-wake solution may then be applied directly as input to the far-wake analysis. Until such time, the present analysis, which treats the far wake, is useful to determine the nature of coupled chemical and diffusion processes for assumed initial conditions.

Analysis**

The diffusion of species for axisymmetric ($m = 1$) or two-dimensional ($m = 0$) wake flow may be described by the

‡ Important for half-cone angles of about 20° or greater.

§ Recently, numerical finite-difference methods for blunt-body flows, taking into account vorticity swallowing, have been developed by H. Li of the General Electric Co. and S. Zeiberg of General Applied Science Laboratories.

¶ It should be emphasized that, although detailed numerical analyses of the laminar wake have been reported,[9, 10, 13] the pressure interaction between the viscous and inviscid flows was ignored in these calculations. Since it is this interaction that actually determines the solution in the near-wake region,[14, 15] the usefulness in the near wake of analyses, such as those reported in Refs. 9, 10, and 13, is uncertain. By near wake, the region behind the body, which includes the Crocco-Lees critical point and over which the wake recompression takes place, is referred to; this region may extend well beyond axis velocity ratios[16] of the order of 0.3.

** The notation used here is generally the same as that of Ref. 5.

boundary-layer form of the species conservation equation

$$\rho u \frac{\partial \alpha_i}{\partial x} + \rho v \frac{\partial \alpha_i}{\partial y} = \frac{1}{y^m} \frac{\partial}{\partial y} \left(\frac{\epsilon}{d} \rho y^m \frac{\partial \alpha_i}{\partial y} \right) + \dot{\omega}_i d \qquad (1)$$

and the over-all continuity relation

$$(\partial/\partial x)(\rho u y^m) + (\partial/\partial y)(\rho v y^m) = 0 \qquad (2)$$

In the preceding, ϵ is the local (turbulent) diffusivity, $\dot{\omega}_i$ represents local species production by reaction, and all of the length scales have been normalized by d. As in Ref. 5, the Howarth-Dorodnitsyn transformation is used to define a new lateral scale Y_T for the turbulent wake

$$\rho y^m dy = \rho_f Y_T{}^m dY_T \qquad (3)$$

where the subscript f denotes quantities at the edge of the wake. Also, a scale for the inviscid wake is defined by

$$\rho_L y^m dy = \rho_\infty Y^m dY \qquad (4)$$

The species mass fractions are assumed to be distributed as

$$(\alpha_i - \alpha_{i_f})/(\alpha_{i_0} - \alpha_{i_f}) = \beta_i(x) G(\theta_i) \qquad \theta_i = Y_T/Y_{s_i}(x) \qquad (5)$$

so that $\beta_i(0) = 1$, $G(0) = 1$, and $G(\theta_i) = 0$ for $\theta_i \geq \theta_{i_f} = Y_{T_f}/Y_{s_i}$. The constant quantities α_{i_0} are assumed to be known, and they denote the initial species mass fractions on the axis; the variables $\alpha_{i_f}(x)$ are either assumed known or are simultaneously calculated and denote the inviscid species at the edge of the wake. Thus, two parameters $\beta_i(x)$ and $Y_{s_i}(x)$ are used to represent the species in the wake. The first, β_i, is the relative axis mass fraction; the second, Y_{s_i}, is a characteristic mass thickness parameter. This parameter is introduced to allow the profiles to adjust their flatness as the diffusion proceeds. The profile $G(\theta_i)$ is assumed.†† Solving (2) for v, inserting into (1), integrating over the wake using (3–5), and assuming $u \approx u_f \approx u_\infty$ gives a relation for dY_{s_i}/dx that is conveniently written in terms of θ_{i_f} as

$$(m+1)\theta_{i_f}{}^{-1}\theta_{i_f}{}' = -[1 - (m+1)^{-1}\beta_i{}^{-1}P_i{}^{-1}] \times (\alpha_{i_0} - \alpha_{i_f})^{-1}\alpha_{i_f}{}' + (m+1)Y_f{}^{-1}Y_f{}' + \beta_i{}^{-1}\beta_i{}' - [\beta_i{}^{-1}d/(\alpha_{i_0} - \alpha_{i_f})u_\infty](\varphi_i/P_i) \qquad (6)$$

where

$$P_i = \int_0^1 G(\theta_{i_f}\zeta)\zeta^m d\zeta$$

$$\varphi_i = \int_0^1 \frac{\dot{\omega}_i}{\rho} \zeta^m d\zeta \qquad \zeta = Y_T/Y_{T_f}$$

and the first term on the right-hand side represents the effect of reactions in the inviscid outer region. Also, use of (3–5) in (1) gives, on the axis,

$$\beta_i{}' = -(1 - \beta_i)(\alpha_{i_0} - \alpha_{i_f})^{-1}\alpha_{i_f}{}' + (m+1)G''(0)\beta_i(\theta_{i_f}{}^2/Y_{T_f}{}^2)(\tilde{\epsilon}/u_\infty d) + [(\alpha_{i_0} - \alpha_{i_f})^{-1}/\rho(x, 0)](d/u_\infty)\dot{\omega}_i(x, 0) \qquad (7)$$

As in the notation of Ref. 5,

$$\tilde{\epsilon} = [\rho(x, 0)/\rho_f]^{2/(m+1)}\epsilon$$

The form used here for ϵ is identical to that assumed in Refs. 5 [Eq. (10b)] and 17 since, as discussed later, calculations using this form seem to agree well with experimental data. The effective turbulent Lewis number is thereby assumed to be unity.

Eqs. (6) and (7) constitute a set of relations enabling the species parameters β_i and Y_{s_i} to be calculated by integration, provided that the thermal state and the width of the wake are known. These quantities may be obtained by only a slight modification of the Lees-Hromas method. This modification consists simply in replacing the approximate equation of state $p \sim \rho h$ used therein with the exact one, namely,

$$p = \rho(R_0/\overline{\mathfrak{M}})T \qquad \overline{\mathfrak{M}}^{-1} = \sum_i \alpha_i \mathfrak{M}_i{}^{-1}$$

With this simple modification, the integration of Eqs. (6) and (7) may be carried out simultaneously with the integration of Eq. (38) of Ref. 5 for Y_f.‡‡ For the molecular specific heats, linear vibrators are assumed, with the vibration in equilibrium. The atomic specific heats are assumed constant. These assumptions seem appropriate for the range of temperatures involved.

To obtain the inviscid species concentrations α_{i_f}, a simultaneous integration along the inviscid streamlines intersected by the turbulent wake is required. With a pressure field determined from an appropriate characteristics solution for the inviscid flow and a given initial radial distribution, this integration becomes a straightforward procedure.

Ionization Kinetics

For the neutral air species in the reacting wake, the more or less standard set of reactions listed in the Appendix has been employed. The rate constants used for all of the reactions considered are given in Table 1.

For the charged air species, the reaction set G-L given in the Appendix has been chosen to represent the ionization kinetics. This set is, of course, far from complete but represents what the authors believe to be the most significant types of reactions involved. Reaction G is the well-known associative ionization-dissociative recombination reaction, which dominates the removal of electrons at low air density and high electron concentration.[6] Both of the attachment reactions H and I are considered since either may be significant mechanisms for electron removal. The electron affinity of O (~1.5 ev) enables earlier attachment than for O_2 which has a lower affinity (~0.5 ev). However, unless highly dissociated at the beginning of the wake, the usually smaller atomic oxygen concentration may prohibit significant electron removal by O, especially in the far downstream wake, which is mainly molecular.[6] Although the neutralization reactions J and K are important in the early, high-temperature part of the wake, they contribute little once the temperature is reduced since the forward rates vary as the square of the charge density, and the backward reactions require large activation energies. The charge exchange reaction L may play a significant role in removing O_2^- depending on whether this reaction proceeds as a simple recombination reaction, or whether an activation energy is required.[8] This fact seems to have been overlooked in other recent analyses. The presence of positive atomic ions and radiative processes has been ignored in the ionization model. This assumption

†† Studies have been made of the effect of profile shape in the present method. A comparison of calculations for the parabolic shape $G(\nu) = 1 - \nu^2$ and the cosine distribution $G(\nu) = \frac{1}{2}(1 + \cos\pi\nu)$ for a given value of the diffusivity constant $KG''(0)$ indicates very close agreement in all of the quantities calculated and, therefore, a lack of sensitivity to the specific profile chosen.

‡‡ In Ref. 5 a fictitious inviscid profile between $y = 0$ and $y = y_f$ was employed. The variable Y_f was calculated for this profile and related to Y_{T_f} by introducing a quantity δ to account for the displacement effect of the turbulent wake. It has been pointed out by A. G. Hammitt that, since the variable Y is essentially a mass flux coordinate (ignoring the fact that the velocity is not quite uniform), by equating $Y_f{}^{m+1}$ with $(\rho_f/\rho_\infty) \cdot Y_{T_f}{}^{m+1}$, and by carrying out the solution entirely in mass flux coordinates, the use of a fictitious profile may be avoided. The Y coordinate is then interpreted as the mass flux coordinate for the actual physical flow, rather than for a fictitious inviscid flow.

s believed to be applicable to the majority of the wake for flight speeds at or below typical re-entry vehicle velocities.

An important, yet imperfectly understood, question in chemical kinetic calculations for turbulent flows is the applicability of quasi-steady or laminar expressions to represent[11, 18, 19] the species reaction terms $\dot{\omega}_i$. At least two crucial questions are involved, namely, 1) the degree of homogeneity of the flow field, and 2) the use of a mean temperature to characterize the local thermal energy of the flow. As previously mentioned, the present homogeneous mixing model assumes instantaneous development of an equilibrium turbulent structure in the mass entrained by the wake. With regard to the influence of temperature fluctuations on the reaction processes, it has been suggested (for example, Ref. 18) that, as long as the energy content of the fluctuations is small compared with the average static enthalpy, the molecular collision processes may remain unaffected. This criterion is certainly an upper limit. More stringent criteria are probably actually required to insure the validity of the use of quasi-steady kinetic rate expressions. However, an important point relative to turbulent nonequilibrium far wakes is that the chemical processes occurring are predominantly exothermic. Hence the dependence of the chemical rates on temperature is weak. This situation is in direct contrast to the turbulent boundary layer or perhaps the near wake, both of which are usually endothermic with rates exponentially dependent on temperature. Use of quasi-steady rates for these turbulent flows thus appears more questionable than for the far wake. As pointed out in Ref. 10, use of the quasi-steady assumption should be construed more as a reference to the state of the art on the subject rather than as a belief in the correctness of this assumption.

Explicit Solutions for Turbulent Wake Species

Since the problem has been reduced to a set of simultaneous first-order differential equations, provided that $p(x)$ is assumed, numerical solutions may be obtained with the aid of a digital computer. Examples of such solutions are given in a later section. However, it is helpful to have explicit solutions wherever possible. By the use of further simplifying assumptions, several new explicit solutions have been obtained and are discussed briefly in the next few sections.

Pure Diffusion

Taking $\dot{\omega}_i = 0$, $\alpha_{i_f}' = 0$ in (7) and (8) gives, on integration,

$$\left.\begin{aligned} \theta_{i_{f_0}}{}^{-1}\theta_{i_f} &= Y_{f_0}{}^{-1}Y_f\beta_i{}^{1/(m+1)} \\ \beta_i &= \left[1 + 2G''(0)\,\frac{\theta_{i_{f_0}}{}^2}{Y_{f_0}{}^2}\int_{x_0}\frac{\tilde{\epsilon}}{u_\infty d}\times \left(\frac{\rho_f}{\rho_\infty}\right)^{2/(m+1)} dx\right]^{-(m+1)/2} \end{aligned}\right\} \quad (8)$$

To obtain further simplification, it is assumed that the entire inviscid drag is contained within the wake; then the wake growth obeys a simple power law. For example,[20] for an axisymmetric body ($m = 1$),

$$\left.\begin{aligned} Y_f/Y_{f_0} &= \chi^{1/3} \\ 2G''(0)(\tilde{\epsilon}/u_\infty d)\,Y_f{}^{-2} &= \tfrac{2}{3}\Lambda\chi^{-1} \\ T/T_\infty &= 1 + \Lambda_1\chi^{-2/3} \end{aligned}\right\} \quad (9)$$

Table 1 Reaction rate table[a]

Catalyst, M	Reaction[b]	a_f	b_f	n_f	a_b	b_b	n_b
1	A	0.276E17[c]	0	−0.5	0.502E18	0.113E6	−0.5
2		0.109E17		−0.5	0.198E18		−0.5
3		0.109E17		−0.5	0.198E18		−0.5
4		0.236E22		−1.5	0.429E23		−1.5
5	A	0.109E17	0	−0.5	0.198E18	0.113E6	−0.5
1	B	0.617E16	0	−0.5	0.103E18	0.594E5	−0.5
2		0.799E20		−1.5	0.133E22		−1.5
3		0.301E16		−0.5	0.502E17		−0.5
4		0.301E16		−0.5	0.502E17		−0.5
5	B	0.225E21	0	−1.5	0.375E22	0.594E5	−1.5
1	C	0.102E21	0	−1.5	0.408E21	0.755E5	−1.5
2		0.102E21			0.408E21		
3		0.200E22			0.800E22		
4		0.102E21			0.408E21		
5	C	0.102E21	0	−1.5	0.408E21	0.755E5	−1.5
...	D	0.133E11	0.356E4	1.0	0.319E10	0.197E5	1.0
...	E	0.163E14	0	0	0.741E14	0.378E5	0
...	F	0.241E24	0.430E5	−2.5	0.456E25	0.646E5	−2.5
...	G	0.181E22	0	−1.5	0.302E14	0.325E5	−0.5
1	H	0.100E17	0	0	0.600E8	0.533E4	1.5
2		0.100E19			0.600E10		
3		0.100E17			0.600E8		
4		0.100E17			0.600E8		
5	H	0.100E17	0	0	0.600E8	0.533E4	1.5
1	I	0.110E20	0	−1.0	0.112E12	0.162E5	0.5
2							
3							
4							
5	I	0.110E20	0	−1.0	0.112E12	0.162E5	0.5
...	J	0.100E19	0	−0.5	0.653E19	0.918E5	−1.0
...	K	0.100E19	0	−0.5	0.111E20	0.103E6	−1.0
...	L	0.122E13	0.533E4	0.5	0.208E13	0.162E5	0.5

[a] Reaction rate constants (see Refs. 35–38 for sources):

Forward rate $k_f = a_f T^{n_f} \exp\{-b_f/T\}$

Backward rate $k_b = a_b T^{n_b} \exp\{-b_b/T\}$

[b] Units: $(\text{cm}^3/\text{g-mole})^n\,\text{sec}^{-1}$, where n is the reaction order; the temperature must be expressed in °K.

[c] The numerical exponent symbol E is standard formula translation (Fortran) notation (e.g., 0.1E10 means 0.1×10^{10}).

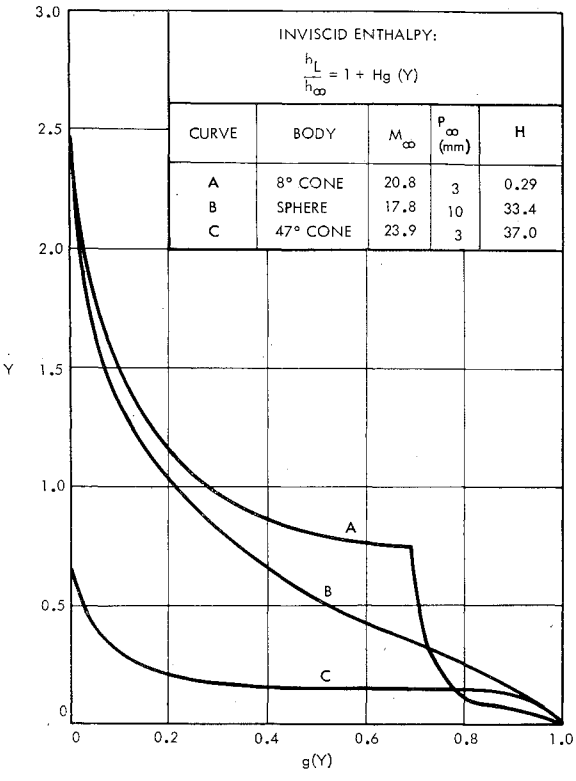

Fig. 1 Inviscid enthalpy distribution.

wherein

$$\Lambda = -\frac{3}{16}\frac{G''(0)}{G_1}\frac{KC_D}{Y_{f_0}^3} \qquad \Lambda_1 = \frac{(\gamma_\infty - 1)}{16G_1} M_\infty^2 \frac{C_D}{Y_{f_0}^2}$$

$$\chi = 1 + \Lambda(x - x_0)$$

Inserting the foregoing into (8) gives

$$\beta_i^{-1} = 1 + \theta_{if_0}^2(\chi^{2/3} - 1) \qquad \theta_{if} = \theta_{if_0}\chi^{1/3}\beta_i^{1/2}$$

Thus, at small x for $\theta_{if_0} < 1$, the particle density on the wake axis n_i increases and the characteristic species scale Y_{s_i} decreases. The converse is true for $\theta_{if_0} > 1$. At large distance

$$n_i/n_{i_0} \approx (\Lambda_1/\theta_{if_0}^2)(\Lambda x)^{-2/3} \qquad \theta_{if} \approx 1$$

Further, at all distances when $\theta_{if_0} = 1$,

$$n_i/n_{i_0} = (1 + \Lambda_1^{-1}\chi^{2/3})^{-1} \qquad \theta_{if} = 1$$

The physical explanation of these simple results is clear. Since the diffusion is turbulent with equal mass and energy diffusivities ($Le = 1$), the species concentrations in the absence of reactions diffuse exactly as the enthalpy does. The species have the over-all constraint of constant total particle number over the wake; the enthalpy has the constraint of constant drag within the wake. Thus, if the initial density distribution is flatter than the enthalpy distribution (i.e., if $\theta_{if_0} < 1$), the species distribution will tend to become sharper as the wake growth commences, and the axis concentration will increase. The converse is true for an initially sharper species distribution. In the limit of large distance, the species and enthalpy distributions become identical ($\theta_{if} = 1$) and the axis concentration obeys the well-known $\frac{2}{3}$ power law. The chemical production of species in the wake will certainly modify this process. Although electron decay processes in the wake are generally rapid relative to diffusion, the recombination of atoms is generally slow. Consequently, the pure diffusion case studied previously may be a valid approximation for the atomic species, but is significantly modified by chemical kinetic effects for the electron density.

Atom Recombination with Coupled Diffusion

Further simple solutions may be obtained if only one species parameter is considered. Taking $\theta_{if} = 1$ in either (6) or (7) will yield an immediate solution if $\dot{\omega}_i$ is sufficiently simple. For example, for the recombination of atoms,

$$\dot{\omega}_A = -4k_{r_A}(\rho^3/\mathfrak{M}^2)\alpha_A^2 \tag{10}$$

wherein a factor $1 + \alpha_A$ has been replaced by unity since $\alpha_A \ll 1$. Inserting (10) into (7) with $\theta_{if} = 1$ gives, on integration,

$$\alpha_A^{-1} = f_A(x)\left[\alpha_{A_0}^{-1} + \int_{x_0} A_1(x)f_A^{-1}(x)dx\right] \tag{11}$$

where

$$A(x) = \frac{2G''(0)}{Y_{T_f}^2}\frac{\tilde{\epsilon}}{u_\infty d} \qquad A_1(x) = \frac{4}{\mathfrak{M}^2}\frac{\rho_\infty^2 d}{u_\infty}\frac{\rho^2(0,x)}{\rho_\infty^2}k_{r_A}$$

$$f_A(x) = \exp\{-\int A(x)dx\}$$

To simplify further, a specific reaction rate $k_{r_A} = a_{r_A}T^{-3/2}$ is assumed and the relations [Eq. (9)] are applied. Then with $\rho \sim T^{-1}$,

$$\alpha_A^{-1} = \chi^{2/3}\left[\alpha_{A_0}^{-1} + \frac{3}{2}\frac{\lambda_A}{\Lambda}\int_1^{\chi^{2/3}} \nu^3(\Lambda_1 + \nu)^{-7/2}d\nu\right]$$

where

$$\lambda_A = (4a_{r_A}/T_\infty^{3/2}\mathfrak{M}^2)(\rho_\infty^2 d/u_\infty)$$

The integral is readily evaluated; for $x \gg \Lambda^{-1}$,

$$\alpha_A^{-1} \approx (\Lambda x)^{2/3}[\alpha_{A_0}^{-1} + (3\lambda_A/\Lambda)(\Lambda x)^{1/3}] \tag{12}$$

Thus, the atom concentration diffuses as $x^{-2/3}$ and recombines as x^{-1}. The recombination will exceed the diffusion for distances greater than $x_{D_A} = \Lambda^2(3\alpha_{A_0}\lambda_A)^{-3}$. With $a_{r_A} \approx 10^{19}$, and since $\Lambda^2 \approx 10^{-3}\ C_D^{-1}\ T/T_f$, then for a typical value $\alpha_{A_0}^{-3}C_D^{-1}T_\infty/T_f = 10^2$, and with $U_\infty/d = 10^4$ sec^{-1}, there results $x_{D_A} \approx 10^{-30}\rho_\infty$($\rho_\infty$ in g/cm^3). Thus, at about 100 kft altitude and below, recombination becomes the dominant process for the decay of the axis atom concentration, and a linear decay with distance is predicted. Above this altitude, the atom concentration is dominated by diffusion.

Electron Recombination, Attachment, and Diffusion

A solution for the electron decay process may be obtained in the same fashion. Considering only electron recombination and attachment to molecular oxygen,

$$\dot{\omega}_e/\mathfrak{M}_e = -k_{r_e}n_e^2 - k_a n_{O_2}^2 n_e$$

and inserting into (7) gives, upon integration,

$$n_e^{-1} = \frac{\rho_0}{\rho(x,0)}f_e(x)\left[n_{e_0}^{-1} + \int_{x_0} A_2(x)f_e^{-1}(x)dx\right]$$

where

$$A_2(x) = (d/u_\infty)k_{r_e}(\rho(x,0)/\rho_0) \qquad A_3(x) = (d/u_\infty)k_a n_{O_2}^2$$

$$f_e(x) = \exp\left[-\int_{x_0}(A - A_3)dx\right]$$

This result is directly analogous to that which Lees[6] originally obtained by applying an integral equation across the wake rather than along the wake axis. With the wake growth

given by (9), and taking $k_{r_e} = a_{r_e}T^{-3/2}$, k_a = const, and $\rho \sim T^{-1}$, then

$$n_e^{-1} = \frac{1 + \Lambda_1\chi^{-2/3}}{1 + \Lambda_1} f_e(\chi) \times \left[n_{e_0}^{-1} + \frac{3}{2}\frac{\lambda_{e_r}}{\Lambda}\int_1^{\chi^{2/3}} \frac{f_e^{-1}(\nu^{3/2})\nu^3}{(\Lambda_1 + \nu)^{5/2}}\, d\nu \right]$$

where

$$f_e(\chi) = \chi^{2/3}\exp\left\{\frac{3}{2}\frac{\lambda_a}{\Lambda}\int_1^{\chi^{2/3}} \frac{\nu^{5/2}}{(\Lambda_1 + \nu)^2}\, d\nu\right\}$$

$$\lambda_{e_r} = \frac{a_{r_e}}{T_\infty^{3/2}}(1 + \Lambda_1)\frac{d}{u_\infty} \qquad \lambda_a = k_a\frac{\alpha_{O_2}^2}{\mathfrak{M}^2}\frac{\rho_\infty^2 d}{u_\infty}$$

For $\lambda_a \gg x \gg \Lambda^{-1}$, i.e., at large x but with negligible attachment,

$$n_e^{-1} = \Lambda_1^{-1}(\Lambda x)^{2/3}[n_{e_0}^{-1} + (3\lambda_{e_r}/n_{e_0})(\Lambda x)^{1/3}] \qquad (13)$$

a result similar to (12) for atom recombination. Here, electron recombination prevails over diffusion beyond $x_{D_e} = \Lambda^2(3n_{e_0}\lambda_{e_r})^{-3}$. Taking $a_{r_e} \approx 2 \times 10^{21}$, then, for typical values of $u_\infty/d = 10^4$ sec^{-1}, $C_D^{-1}\, T_\infty/T_f = 10$, and $T_0/T_\infty \approx 10$, there results $x_{D_e} \approx 10^{24}n_{e_0}^{-3}$. It is necessary for the initial electron level n_{e0} to be lower than 10^8 cm^{-3} for diffusion to play a significant role in the electron level decay. However, for a small blunt body with $u_\infty/d = 10^6$ sec^{-1}, $T_0/T_\infty = 20$, and $C_D^{-1}\, T_\infty/T_f = 10^{-1}$, then $x_{D_e} \approx 10^{35}/n_{e_0}^3$, and diffusion dominates much of the wake for initial electron densities as high as 10^{11} cm^{-3}. The strong dependence on the initial electron level and temperature ratio is clear. These quantities increase rapidly with flight speed so that the electron decay behavior in the diffusion-recombination region for small bodies should show large variations as the flight speed is increased. When $x \gg \lambda_a^{-1}$, then

$$n_e \approx n_{e_0}\Lambda_1(\Lambda x)^{-2/3}\exp(-\lambda_a x)$$

and the decay is exponential. With $k_a = 10^{18}$, $\lambda_a = 4 \times 10^{13}\,\rho_\infty d/u_\infty$ and for $u_\infty/d \approx 10^4$ sec^{-1}, then $\lambda_a \approx 4 \times 10^9\,\rho_\infty{}^2$. Therefore, at 100 kft, attachment is significant beyond distances of the order of $x \approx 10$, whereas at 150 kft, a distance of the order of $x \approx 10^3$ is required. However, at $x \approx 10$ behind the body, the wake temperature is still relatively high and the detachment reaction (which has been ignored) will prevent a significant accumulation of O_2^- ions; that is, below 150 kft the attachment-detachment reaction is nearly in equilibrium. When the wake temperature finally falls below some critical level, attachment will then rapidly absorb the remaining electron concentration, leaving only O_2^- and NO^+ in the wake. Thus, for a fully turbulent wake, since the distance x necessary for the wake temperature to fall below the critical attachment temperature is essentially independent of altitude, the final electron cleanup in the wake caused by attachment will occur at about the same x for all of the altitudes below about 150 kft, until the recombination reaction goes into equilibrium.

Numerical Results§§

Detailed numerical calculations are given herein for a variety of body shapes and sizes: a large slender cone, a small 6° cone with several blunt-nose shapes, a large 12°-sphere cone, and a small sphere. The comparison of present results with those of other analyses is made for the large slender cone. The blunt-body shape study is carried out for the small 6° cone with three nose shapes. Wakes with contaminants are calculated for a large blunt body and a large slender body. The calculations of the wakes of a small sphere are for comparison with ballistic range results.

For slender body cases, the inviscid enthalpy and pressure distributions, which are required as an input to the wake solutions, were obtained from an equilibrium characteristics program as discussed in Refs. 5 and 20. For blunt bodies, an equilibrium characteristics solution was used to generate pressure distributions. Then nonequilibrium stream-tube calculations were carried out to determine the rest of the inviscid flow field variables. In Fig. 1, inviscid enthalpy distributions, normalized by the axis value $h_L(0)/h_\infty - 1 \equiv H$ are shown for several of the cases considered. The slender cone distribution is, of course, flat out to the point where the expansion from the cone shoulder intersects the bow stock. The enthalpy then rapidly diminishes to the ambient level at larger streamline distances. Because of nonequilibrium effects, the blunt cone enthalpy varies in the nose region as shown in Fig. 1. Twelve inviscid stream-tubes were calculated in order to define the shape of the profile shown. The nose and base diameters for the 47°–6° biconic shape considered were 2.4 and 9 in., respectively. The base diameter is used to normalize the radial coordinate. Wake pressure distributions, as suggested in Refs. 5 and 20, were employed in the calculations. However, the influence of the assumed variation of pressure in the wake is actually confined to a very short distance downstream.¶¶

Slender Cone, Comparison with Other Methods*

For sufficiently slender bodies, temperatures in the inviscid flow are inadequate for the generation of appreciable ionization or dissociation phenomena; thus, the nviscid flow is nonreacting. A typical case of this kind has been considered: an 8° cone of 2.82-ft diam at $U_\infty = 22$ kft/sec and 150 kft altitude. Recent experimental data indicate that the flow near the wake neck of such a slender body may be stable over a large range of Reynolds number and that the transition location moves toward the neck with increasing Reynolds number.[13, 23–25] A length of laminar run may therefore precede the turbulent wake, provided that the Reynolds number is not so large that the body flow or free-shear layer flow before the neck is turbulent. The exact conditions under which the upstream flow becomes turbulent depend on details such as angle of attack, ablation effects, and wall temperature and roughness, and are difficult to predict precisely. However, a transition location was estimated, using the laboratory data correlation of Ref. 13.

Species concentrations for the laminar run were calculated along the axis and several other streamlines by using a one-dimensional, reacting streamline model. The initial composition of the gas at the start of the laminar run as well as the stagnation enthalpy and velocity history for the laminar

§§ The computer program was written for an IBM 7094 by Maureen L. Sprankle. A standard Adams-Moulton-Runge Kutta (AMRK) predictor-corrector routine was used for some of the cases given. For others, a method recently suggested by Treanor[21] was applied; the latter appears to improve calculation time significantly in near-equilibrium cases. An attempt to improve upon the Treanor method for a coupled set of species is currently being pursued.

¶¶ The enthalpies given in Fig. 1 were found at the $p = 4\,p_\infty$ station.

* Results from the present theory are compared here with results obtained by the methods given in Refs. 9 and 10 and with unpublished calculations of H. Li of the General Electric Co. The last two are finite difference calculations. The method of Ref. 9 is a strip method for laminar flow and an integral method for turbulent flow (previously discussed). By agreement, the same initial conditions for the laminar run were assumed for each method. However, each group performing the calculations made its own estimate of the location of transition. The authors wish to thank A. Pallone of Avco, W. Daskin of General Applied Science Labs., Inc., and H. Lew of the General Electric Co. for making these calculations available. They were initially reported in part in Ref. 22.

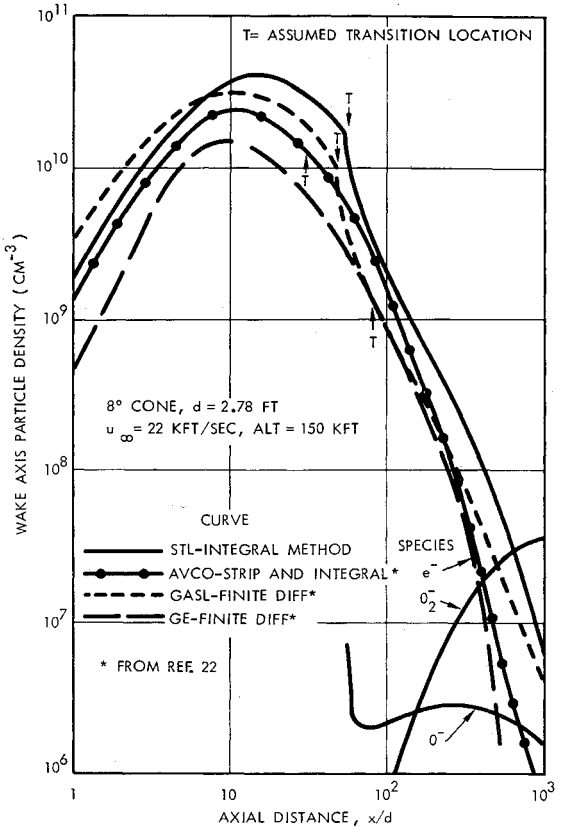

Fig. 2 Axis charged particle concentrations, slender cone.

streamlines were taken from estimates for these quantities made by A. Pallone.† The initial enthalpy ratio used, $h(0)/H_\infty = 0.30$, is of the order indicated by applying to the near wake the approximate model of Chapman,[26] as modified by Denison and Baum.[27] As shown in Fig. 2, a comparison of electron density obtained by the detailed laminar calculations of Zeiberg, Lien, and Li indicates that the chemical processes determined by the present simple method closely reproduce results obtained by these detailed calculations. Thus, the principal effect of the short laminar run is to allow time for chemical reactions to proceed, and then near-equilibrium species concentrations will result. At the estimated location of the transition point, the laminar streamline properties there were used to determine levels and distributions for the turbulent wake calculation. The axis velocity ratio at this point was $u/u_\infty = 0.6$. Hence several diameters would actually be required for the rapid turbulent diffusion to raise this ratio to the assumed value of near unity (see the section on "Comparison with Experiment"). The resulting axis-charged particle concentrations calculated for the turbulent wake are also given in Fig. 2. The attachment of electrons to atomic oxygen is seen to begin before an x/d of about 10^2 and, later, to molecular oxygen just beyond this distance where the temperature is low enough (below about 800°K) to permit stable O_2^- ions. The familiar linear recombination decay with distance predominates at smaller distances, except for an even sharper drop in electron concentration immediately after transition. This drop is particularly noticeable in the present calculations and in those of Zeiberg. It is so because the effective thickness of the electron distribution is initially smaller than the enthalpy thickness at the transition point; beyond this point the electrons then rapidly diffuse outward to the edge of the wake, and the axis concentration is lowered. The agreement between the various theoretical methods is reasonably good over the entire range of the calculation.

† See preceding footnote on page 831.

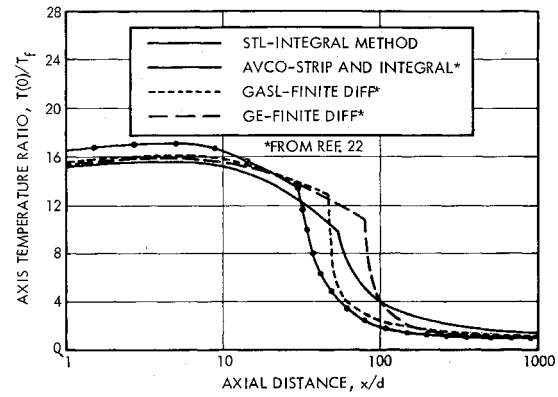

Fig. 3 Temperature on wake axis, slender cone.

The temperature calculated for the axis of the wake is shown in Fig. 3. Although the temperature decrease shown for the turbulent wake is quite rapid in comparison with the laminar result, nevertheless, temperature levels as high as 1000°K still exist at 100 body diameters downstream. Beyond 500 diameters, the wake intercepts the inviscid streamline from the expansion-shock wave intersection point, and a slightly more rapid temperature decrease then results as the wake mixes with the colder inviscid fluid. The divergence among the various theoretical methods appears to exist mainly because somewhat different estimates were made for the location of transition in each calculation.‡ Thus, accidentally, these results indicate the effect of transition location on the axis temperature history.

Axis mass fractions for N, O, and NO are shown in Fig. 4 for the present calculations. The N concentration rapidly diminishes in the turbulent wake because of the rapid NO shuffle reactions as the temperature is lowered. However, the O concentration disappears mainly by simple diffusion, as previously suggested by the order-of-magnitude estimates of the extent of the diffusion-controlled vs recombination-controlled wake given by the explicit solutions.

In Fig. 5 mean electron-density contours are shown. Note that the electron attachment to molecular oxygen near the low-temperature edge of the wake results in an elec-

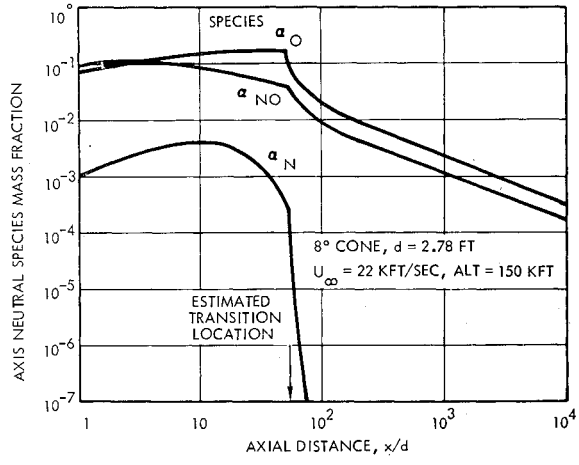

Fig. 4 Axis mass fraction for neutral species, slender cone.

‡ Comparisons of the theoretical methods were also carried out at 100 kft altitude for a completely turbulent wake.[22] In these calculations, the temperature levels, as well as electron levels, agreed quite well among the various methods.

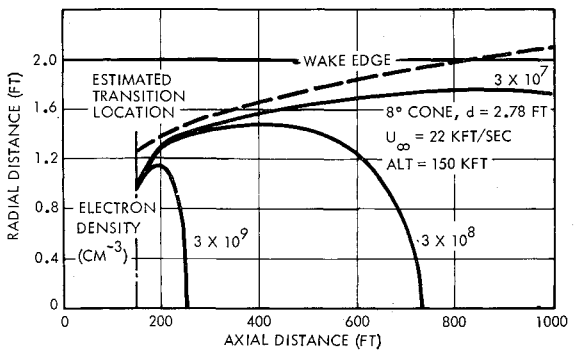

Fig. 5 Mean electron-density contours for slender cone wake.

tron-distribution width significantly smaller than the wake width. This effect is necessarily confined to the low electron-level region of the wake. A simple one-parameter integral method does not allow the calculation of such effects. However, they are reasonably represented in the present method.

Blunt-Nosed Cone

Three different blunt-cone shapes were considered as shown in Fig. 6: 1) a sphere cone, 2) a flat-faced cone, and 3) a 47°–6° biconic shape. The nose radii were taken so that the estimated over-all drag coefficients were the same. The inviscid, blunt-cone flow fields contain dissociated and ionized species up to the radial stream coordinate where the shoulder expansion reduces the shock strength. The production of these species is cut off at the shoulder by the expansion, and the partially ionized and dissociated gas there (which is nearly frozen because of the low pressure and high velocity) then forms the inviscid wake. For example, in Fig. 7 the radial distributions of a_O, a_N, a_{NO} and temperature in the inviscid flow field at the start of the wake calculations for the 47°–6° biconic shape are shown.§ These

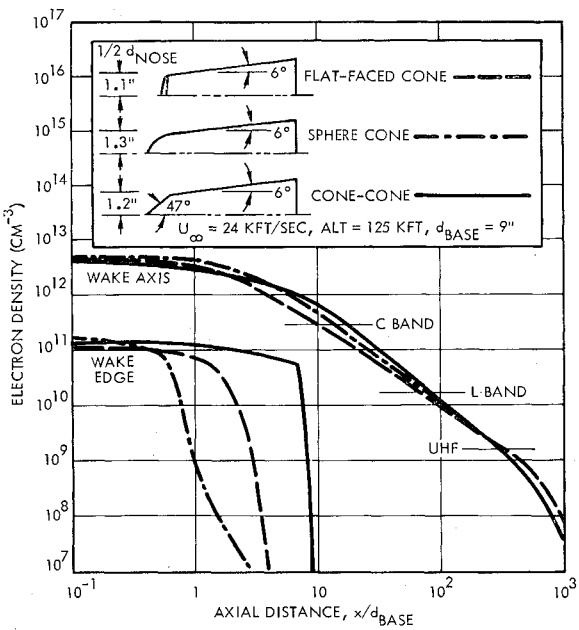

Fig. 6 Axis electron density for blunt-nosed cones.

§ The large gradients in the supposed inviscid flow at the shoulder expansion-shock intersection will certainly cause a smearing out of these profiles by molecular diffusion in the actual physical case. However, over lengths of interest, this effect is probably small.

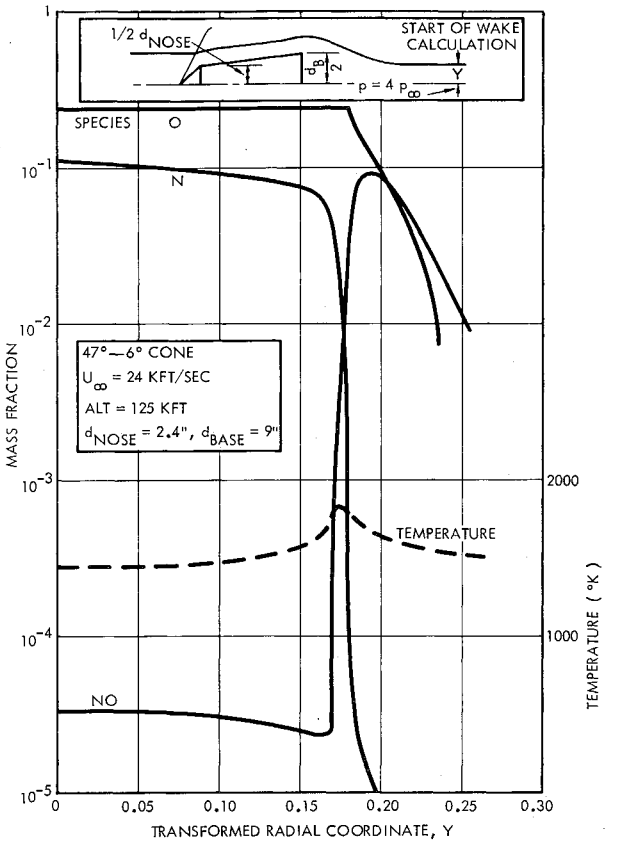

Fig. 7 Mass fraction and temperature of the initial inviscid species, biconic shape.

values occurred at the point where $p/p_\infty = 4$. With this distribution as a starting condition, along with the values of the other species in the inviscid flow, the behavior of the turbulent wake growing into the dissociated, ionized, and reacting inviscid field of this blunt body was calculated. Although not shown, the inviscid flow fields for the other two blunt shapes were similarly determined and used as initial conditions for the turbulent wake calculation of these bodies.

Shown in Fig. 8 are the resulting turbulent axis and wake edge temperature for the biconic configuration; an initial axis value $h(0)/H_s = 0.6$ was assumed.¶ Figure 6 shows the axis and edge electron concentrations for all of the three blunt-nose shapes studied. The axis values in the turbulent wake were assumed to be in equilibrium at the initial station. The effect of the reacting inviscid flow in maintaining a high electron concentration, until the shoulder-expansion, fan-shock-wave intersection streamline is reached, is apparent. The irregular behavior of the edge temperature as shown in Fig. 8 results from chemical kinetic effects at the shock-wave, shoulder-expansion intersection region, and is also apparent in Fig. 7. Each shape considered had the same inviscid drag coefficient. However, the momentum defect is spread out to a larger radial distance by the conical nose shape. Hence high electron concentrations are maintained farther downstream for this shape.[20] At lower alti-

¶ Nonequilibrium stream-tube calculations of the inviscid flow field for the spheres and blunt cones discussed here have yielded enthalpy ratios h/H_s in the inviscid flow field near the wake axis, varying from 0.5 to 0.6. As a result, somewhat higher initial enthalpy ratios have been chosen for the viscous wake calculations of blunt bodies compared to the values assumed for slender body calculations. Fortunately, the properties of blunt-body wakes are relatively insensitive to the initial enthalpy ratio chosen.

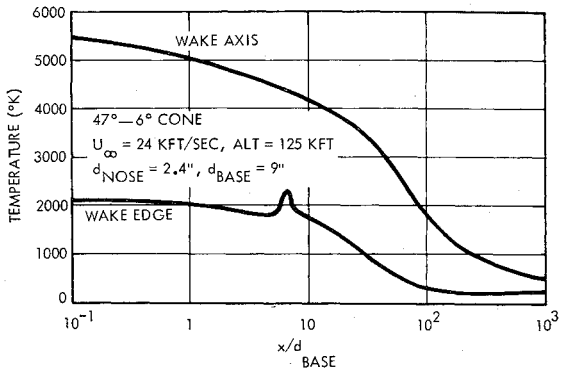

Fig. 8 Wake axis and edge temperatures, biconic shape.

tudes, where the core drag is initially a smaller fraction of the over-all drag, the cone wakes are even longer in comparison with the other bodies.

Contaminated Wakes

The almost universal presence of trace amounts of low ionization potential substances, such as sodium in the materials ablating from high-speed bodies, insure the generation of high electron concentrations in the flow field, even at low ambient pressure. Since this ablating material may well cause a significant extension of the electron trail length, it is of interest to estimate the effect of the contaminant on the electron-density history in the wake. For this purpose, the following reactions have been added to the chemical kinetic set**:

$$Na^+ + e^- + X \rightleftharpoons Na + X$$
$$Na + O + O \rightleftharpoons O_2 + Na^+ + e^-$$
$$Na^+ + O^- \rightleftharpoons Na + O$$
$$Na^+ + O_2^- \rightleftharpoons Na + O_2$$
$$Na + NO^+ \rightleftharpoons Na^+ + NO$$

Some of the chemical rates for the foregoing reactions have been measured, others only estimated. The values used here were taken from the recent survey report by Bortner.[28] Based on these values, the preceding reactions are believed to be the most important.

Calculations were carried out for the contaminated wakes of a slender and a blunt body and compared with pure air results for the same cases. As before, $Le = 1$ has been assumed for all species in the turbulent wake. Bortner[28] and others[29,30] have found that, primarily because of the $Na^+ + O$ — neutralization reaction, followed by the collisional detachment of the electron from O^-, the sodium will produce equilibrium ionization levels both in the boundary layer and laminar run at 150 kft altitude. Thus, the level of electrons obtained depends only on the level of contaminants present in the heat shield. Typical values, which have been measured,[29] are 10–100 ppm. For the present calculations, initial mass fractions in the wake of 10^{-5} and 10^{-6} (heat shield level diluted by a factor of 10) were assumed for the sodium, and the sodium was assumed to be 90% ionized. Results are shown in Fig. 9a for a blunt body and in Fig. 9b for a slender body. It is interesting to note that the initial levels of electrons are not altered much for any of the cases calculated. However, the downstream decay is altered significantly for both the blunt and slender bodies. This is because of the slow recombination of the

** Of course, the concentration of any other trace species having similar properties may be determined by the same reaction yet; only the appropriate chemical constants need be altered.

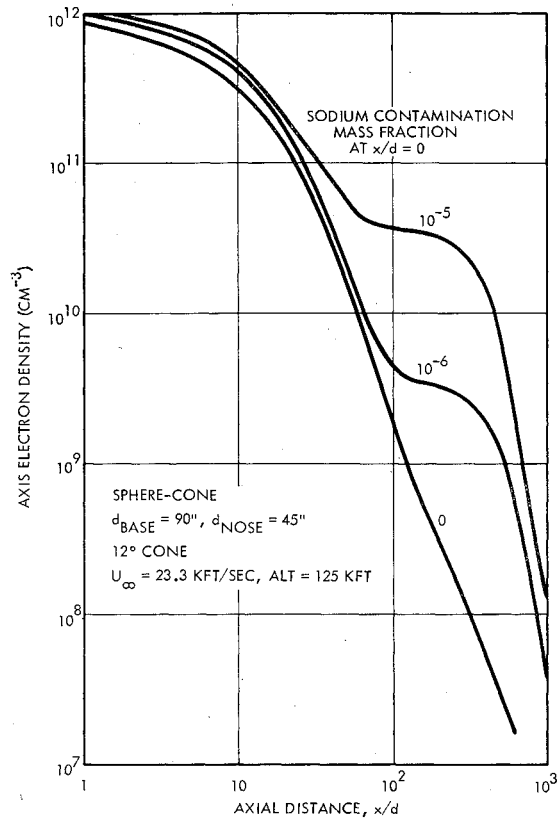

Fig. 9a Axis electron density for blunt-body wake with contaminants.

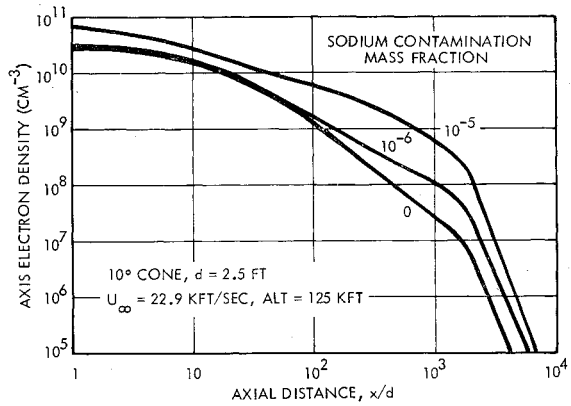

Fig. 9b Axis electron density for slender body wake with contaminants.

sodium electrons until temperatures low enough for oxygen attachment are achieved.

Comparison with Experiment

Wake Velocity

Wake widths calculated by the original Lees-Hromas equilibrium theory[5] have shown excellent agreement with the early (low Mach number) ballistic range data for the small spheres of Slattery and Clay.[25] More recently, Knystautas[31] at the Canadian Armament Research and Development Establishment (CARDE) has confirmed this agreement for sphere sizes as large as 3 in. Strong support is therefore given to the diffusivity model proposed in Refs. 5 and 17. Although measurements of details of hypersonic wakes other than wake width are still scarce, some data on wake velocity are available. Primich[32] has obtained microwave Doppler-shift measurements of the wake velocity of small spheres,

and Washburn, Goldburg, and Melcher[33] have reported measurements of wake velocity, using the luminous streak method. In both cases, the interpretation of the data obtained is not entirely straightforward, yet it is of interest to compare wake velocities calculated by the present theoretical model†† with the experimentally observed results. In Fig. 10, wake velocities, relative to a coordinate system fixed in the laboratory, are plotted vs axial distance for the sphere and cone data referred to. The theoretical curves represent calculated wake axis velocities. These calculations were carried out for conditions representative of the range over which the data were taken. The cone data were taken directly from Fig. 2 of Ref. 33. A comparison of a curve fit of these data with the theory (as well as with that of Ref. 9) has already been given in Ref. 33. The data are included here merely for reference purposes. The sphere data of Primich show a much slower decay than forcones with, again, a reasonable agreement with theory. It is significant that, although the present theory does not calculate the initial low-velocity region correctly, this discrepancy is limited to the first 5–15 diam; thereafter a close agreement with experiment is obtained.

Electron Density

The large variation in inviscid enthalpy results in chemical relaxation processes over a significant portion of the flow behind a sphere. Calculations of this inviscid wake by Lin and Hayes[11] indicate that, for large bodies, the wake may intercept ionized and dissociated species in the inviscid stream as far back as 100 diam behind the body. However, for small bodies, the relatively larger skin-friction drag causes the wake width to begin at a larger value. Farther downstream the outer inviscid flow is essentially molecular in composition, and only kinetics in the turbulent wake need be considered. Calculations for several ballistic firing-range conditions are shown in Figs. 11a and 11b. The data shown were obtained at the Lincoln Laboratory (Massachusetts Institute of Technology), using a resonant cavity technique, which yields linear electron density.‡‡ Although early data[34] evidenced large variations from run to run, apparently because of range contaminants, the experimental difficulties appear to have been overcome, and consistent repeatable data are now available.

Experimental results at 80-mm pressure were first chosen to compare with calculations from the present theoretical model. An enthalpy ratio at $x = 0$ of $h(0)/H_s = 0.5$ was taken and, because of the high temperature associated with this enthalpy level, the initial species concentrations at

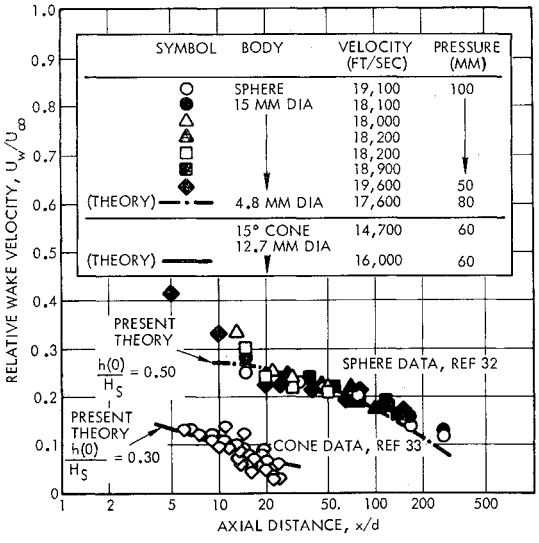

Fig. 10 Wake axis velocities, comparison with experiment.

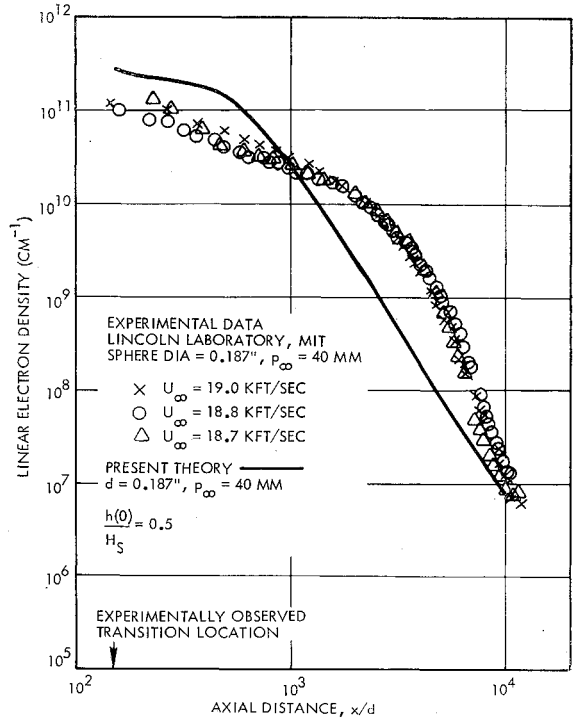

Fig. 11a Linear electron density, comparison with experiment (80-mm pressure).

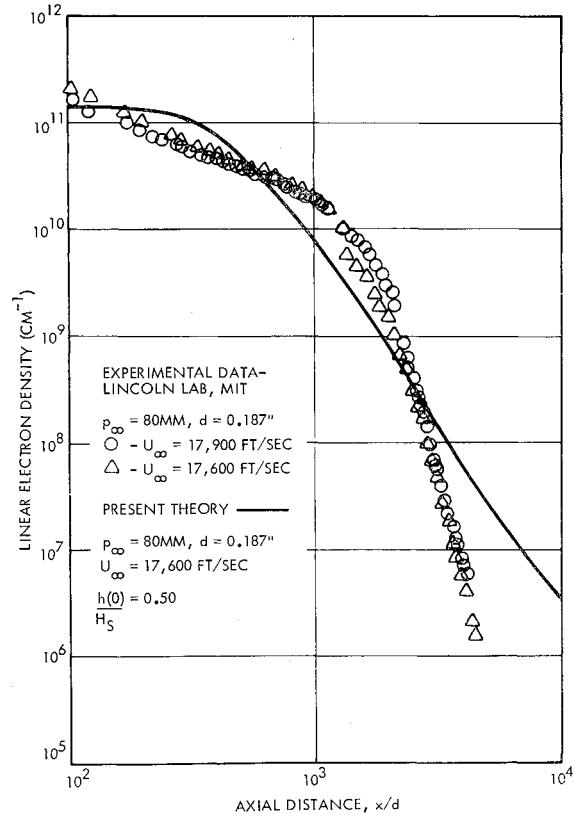

Fig. 11b Linear electron density, comparison with experiment (40-mm pressure).

†† Wake velocities were calculated by simply using the known static enthalpy and the assumption of constant stagnation enthalpy.

‡‡ The authors are indebted to R. Slattery and W. Kornegay of the Lincoln Laboratory, Massachusetts Institute of Technology, for providing this recent unpublished data.

$x = 0$ were taken to be in equilibrium at the local temperature and pressure 4 p_∞. The results of the calculation are shown in Fig. 11a. At 80-mm pressure, available experimental data indicate that transition of the wake should occur within about 20 diam; hence, an entirely turbulent wake was assumed in the calculation. In this case, fair agreement (within a factor of 2) with the measured electron level was obtained, except beyond 5000 diameters, where the experimental results indicate a faster electron decay at lower electron levels than predicted.

A calculation for 40-mm ambient pressure is shown in Fig. 11b. For this case, an estimate of the nonequilibrium laminar run (similar to that just described for the slender cone case) was carried out to the $x/d = 150$ station, which was the estimated transition location. The present method was then applied to the prediction of the electron line density in the far wake. As indicated in Fig. 11b, the procedure described previously appears to overestimate the electron level from 10^2 to 10^3 diam and to underestimate it from 10^3 to 10^4 diam. The disagreement prior to 10^3 is attributable to the necessarily approximate treatment of the laminar wake and the uncertainty in initial conditions. Beyond 10^3 diam, the electron-density history is mainly sensitive to the chemical rates that have been estimated for the cleanup reactions. Specifically, since oxygen attachment dominates the electron removal beyond 10^3 diam, the rates taken for the attachment processes apparently need further study.

Although the agreement of the electron density calculations with experimental measurements is encouraging, a final decision on the accuracy of the theoretical model must await the accumulation and evaluation of more data over a wider range of experimental conditions than is currently available. Measurements of volume density in the wake concurrent with line density results, further independent chemical kinetic measurements of the pertinent reactions discussed herein over a range of temperatures, and additional information on transition and on the distance required for the establishment of a developed turbulent structure would assist in the evaluation of the theory.

Appendix

Species Identification Numbers

1) N_2	6) NO^+
2) O_2	7) e^-
3) NO	8) O^-
4) N	9) O_2^-
5) O	

Neutral Species Reactions

A) $N + N + M \rightleftharpoons N_2 + M$
B) $O + O + M \rightleftharpoons O_2 + M$
C) $N + O + M \rightleftharpoons NO + M$
D) $N + O_2 \rightleftharpoons NO + O$
E) $NO + N \rightleftharpoons N_2 + O$
F) $2\,NO \rightleftharpoons N_2 + O_2$

Charged Species Reactions

G) $NO^+ + e^- \rightleftharpoons N + O$
H) $O_2 + e^- + M \rightleftharpoons O_2^- + M$
I) $O + e^- + M \rightleftharpoons O^- + M$
J) $O^- + NO^+ \rightleftharpoons O + NO$
K) $O_2^- + NO^+ \rightleftharpoons NO + O_2$
L) $O_2^- + O \rightleftharpoons O^- + O_2$

References

[1] Millman, P. W., "An observational survey of meteor trails," ARS Paper 2659-62 (November 1962).

[2] Bloom, M. H. and Steiger, M. H., "Hypersonic axisymmetric wakes including effects of rate chemistry," General Applied Science Labs., Inc., TR 180 (August 1960).

[3] Ting, L. and Libby, P., "Fluid mechanics of axisymmetric wakes behind bodies in hypersonic flow," General Applied Science Labs., Inc., TR 145A (June 1960).

[4] Lykoudis, P., "The growth of the hypersonic turbulent wake behind blunt and slender bodies," Rand Corp., RM-3270-PR (January 1963).

[5] Lees, L. and Hromas, L., "Turbulent diffusion in the wake of a blunt nosed body at hypersonic speeds," Space Technology Labs. Rept. 6110-0004-MU-000 (July 1961); also J. Aerospace Sci. **29**, 976–993 (1962).

[6] Lees, L., "Hypersonic wakes and trails," ARS Paper 2662-62 (November 1962); also AIAA J. **2**, 417–428 (1964).

[7] Bloom, M. H. and Steiger, M. H., "Diffusion and chemical relaxation in free mixing," IAS Paper 63-67 (January 1963).

[8] Webb, W. H. and Hromas, L., "Turbulent diffusion of a reacting gas in the wake of a sharp nosed body at hypersonic speeds," Space Technology Labs. Rept. 6130-6362-RU-000 (April 1963).

[9] Lien, H., Erdos, I., and Pallone, A., "Non-equilibrium wakes with laminar and turbulent transport," AIAA Paper 63-447 (August 1963).

[10] Zeiberg, S. and Bleich, G., "Finite difference calculation of hypersonic wakes," AIAA Paper 63-448 (August 1963); also AIAA J. **2**, 1396 (1964).

[11] Lin, S. C. and Hayes, J. E., "A quasi-one-dimensional model for chemically reacting turbulent wake of hypersonic objects," AIAA Paper 63-449 (August 1963).

[12] Townsend, A. A., *The Structure of Turbulent Shear Flow* (Cambridge University Press, Cambridge, England, 1956) Chap. 7.

[13] Pallone, A., Erdos, H., and Eckerman, J., "Hypersonic laminar wakes and transition studies," AIAA J. **2**, 855–863 (1964).

[14] Crocco, L. and Lees, L., "A mixing theory for the interaction between dissipative flows and nearly isentropic streams," J. Aeronaut. Sci. **19**, 649 (1952).

[15] Lees, L. and Reeves, B., "Supersonic separated and reattaching laminar flows 1. General theory and application to adiabatic boundary layer-shock wave interactions," Graduate Aeronautical Labs., California Institute of Technology Rept. 3 (October 1963).

[16] Webb, W. H., Golik, R. J., and Lees, L., "Preliminary study of the viscous-inviscid interaction in the laminar supersonic near wake," TRW Space Technology Labs. Rept. 6453-6004-KU-000 (July 1964).

[17] Ting, L. and Libby, P., "Remarks on the eddy viscosity in compressible mixing flows," J. Aerospace Sci. **27**, 797–798 (1960).

[18] Ferri, A., Libby, P. A., and Zakkay, V., "Theoretical and experimental investigation of supersonic combustion," Polytechnic Institute of Brooklyn Aerodynamics Lab. Rept. 713 (September 1962).

[19] Corrsin, S., "Statistical behavior of a reacting mixture in isotropic turbulence," Phys. Fluids **1**, 42–47 (January-February 1958).

[20] Hromas, L. and Lees, L., "Effect of nose bluntness on the turbulent hypersonic wake," Space Technology Labs. Rept. 6130-6259-KU-000 (October 1962).

[21] Treanor, C. E., "A method for numerical integration of coupled first order differential equations with greatly different time constants," Cornell Aeronautical Lab. Rept. AG-1729-A-4 (January 1964).

[22] Lien, H., Pallone, A., and Erdos, J., "Comparison and discussion on wake flow field calculations," Avco/RAD TM 64-40 (July 1964).

[23] Webb, W. H., Hromas, L., and Lees, L., "Hypersonic wake transition," AIAA J. **1**, 719–721 (1963).

[24] Demetriades, A., "Hot-wire measurements in the hypersonic wakes of slender bodies," AIAA J. **2**, 245–250 (1964).

[25] Slattery, R. E. and Clay, W. G., "The turbulent wake of hypersonic bodies," ARS Paper 2673-62 (November 1962).

[26] Chapman, D. R., Kuehn, D. M., and Larson, H. K., "Investigation of separated flows in supersonic and subsonic streams with emphasis on the effect of transition," NACA Rept. 1356 (1958); supersedes NACA TN 3869.

[27] Denison, M. and Baum, E., "Compressible free shear layer with finite initial thickness," AIAA J. **1**, 342–349 (1963).

[28] Bortner, M. H., "The chemical kinetics of sodium in reentry," General Electric Co. Rept. 64SD810 (June 1964).

[29] Howard, S., "Application of an approximate boundary layer analysis to nonequilibrium trace species," Space Technology Labs. (to be published).

[30] Lenard, M., "Ionization of cesium and sodium contaminated

air in the hypersonic slender body boundary layer," General Electric Co. Rept. R64SD22 (August 1964).

[31] Knystautas, R., "The growth of the turbulent inner wake behind a 3 inch diameter sphere," Canadian Armament Research and Development Establishment TR 488/64 (February 1964).

[32] Primich, R. and Steinberg, M., "A broad survey of free-flight range measurements from the flow about spheres and cones," General Motors Corp., Defense Research Labs. TR 63-224 (September 1963).

[33] Washburn, W. K., Goldburg, A., and Melcher, B. W., "Hypersonic cone wake velocities obtained from streak pictures," AIAA J. 2, 1465–1467 (1964).

[34] Labitt, M., "The measurement of electron density in the wake of a hypervelocity pellet over a six-magnitude range," Lincoln Laboratory, Massachusetts Institute of Technology (April 1963).

[35] Hall, J. G., Eschenroder, A., and Marrone, P., "Blunt-nose inviscid air flows with coupled non-equilibrium processes," J. Aerospace Sci. 29, 1038–1051 (1962).

[36] Nawrocki, P., "Reaction rates," Geophysics Corp. of America Rept. 61-2-A (1961).

[37] Lin, S. C. and Teare, J. D., "Rate of ionization behind shock waves in air," Avco/Everett Research Rept. 115 (1962).

[38] Chanin, L., Phelps, A., and Biondi, A., "Measurements of the attachment of low-energy electrons to oxygen molecules," Phys. Rev. 128, 219 (1962).

MAY 1965 AIAA JOURNAL VOL. 3, NO. 5

Measured Transition from Laminar to Turbulent Flow and Subsequent Growth of Turbulent Wakes

W. G. Clay,* M. Labitt,† and R. E. Slattery‡
Lincoln Laboratory,§ Massachusetts Institute of Technology, Lexington, Mass.

Turbulent transition distances and growth of turbulent wakes behind $\frac{3}{16}$-in. copper-clad aluminum spheres traveling through rarefied air at 18,000 to 20,000 fps are presented. The data are taken by two independent methods: twin schlieren systems (optical) and a UHF microwave cavity (electronic). The turbulent transition distances are measured to several thousands of sphere diameters at the lower pressures by both methods. Turbulent wake widths are also determined by both techniques and the $\frac{1}{3}$ power growth rate is confirmed for these velocities.

Introduction

OVER the past several years, various measurements of the transition from laminar to turbulent flow in the wake behind various hypervelocity bodies have been reported.[1–3] These measurements, in most cases of direct observation, have been limited to transition occurring quite close to the body, since they have depended either on schlieren or shadowgraph techniques of limited sensitivity or on the observation of rapidly decaying radiation. Indeed, a body of opinion has grown up which considers that transition never occurs further behind a body than approximately 100 body diameters.[4] In order to investigate this problem and several others, new microwave techniques for measuring the width of the electron wake have been developed and combined with improvements in schlieren sensitivity at Lincoln Laboratory. These techniques have permitted the measurement of transition several thousands of body diameters behind hyper-velocity spheres in the ballistic range. In addition, these techniques have been used to measure wake growth by observation of the electron wake and the gas density gradients. The effects of projectile velocity on both of these phenomena have also been investigated and are reported in the paper.

This paper is divided into two parts: techniques and results. In the former, the schlieren and microwave techniques are described; in the latter, the experimental results are presented and discussed.

Measurement Techniques

The schlieren results have been accumulated by utilizing two spark schlieren systems of very high sensitivity which are physically side by side in the same experimental chamber at our larger ballistic range. The systems are completely independent, and the pictures that they take are independently timed from a common trigger pulse that originates when the projectile is in the center of the first schlieren system.

Figure 1 is a sketch of one of the systems being used. It is a double-pass system similar to those previously described by two of the authors[5] but utilizing line spark sources. Each mirror is a 12-in.-diam first-surface sphere of 12-ft radius of curvature. The sensitivity of a schlieren system depends on the focal length of the mirror employed, the number of times the light rays pass through the disturbance being observed, and the size of the light source.[6] Generally, the size of the light source is limited by the requirement that sufficient light be provided to take spark photographs, since the emissivity of the spark plasma remains roughly constant as the size is changed. However, in the case of knife-edge schlieren (as opposed to dot or other nonlinear schlieren obstacles) the results are unaffected by extending the light source parallel to the knife edge. Thus, one may narrow the slit, obtaining improved sensitivity of a smaller source, while the total light intensity is held to the required value by making the source

Received September 8, 1964. The authors are indebted to W. M. Kornegay of Lincoln Laboratory for his helpful suggestions and discussions. We also wish to thank A. P. Ferdinand and J. F. X. Goodwin for their assistance in obtaining and reducing the data reported here.

* Staff Member, Re-Entry Signature Studies Group. Member AIAA.

† Staff Member, PRESS Field Sites.

‡ Associate Leader, Re-Entry Signature Studies Group. Member AIAA.

§ Operated with support from the United States Advanced Research Projects Agency.